Original Research

Wavelet Statistics of Functional MRI Data and the General Linear Model

Karsten Müller, Dr.,* Gabriele Lohmann, Dr., Stefan Zysset, Dr., and D. Yves von Cramon, Prof.

Purpose: To improve the signal-to-noise ratio (SNR) of functional magnetic resonance imaging (fMRI) data, an approach is developed that combines wavelet-based methods with the general linear model.

Materials and Methods: Ruttimann et al. (1) developed a wavelet-based statistical procedure to test wavelet-space partitions for significant wavelet coefficients. Their method is applicable for the detection of differences between images acquired under two experimental conditions using long blocks of stimulation. However, many neuropsychological questions require more complicated event-related paradigms and more experimental conditions. Therefore, in order to apply wavelet-based methods to a wide range of experiments, we present a new approach that is based on the general linear model and wavelet thresholding.

Results: In contrast to a monoresolution filter, the application of the wavelet method increased the SNR and showed a set of clearly dissociable activations. Furthermore, no relevant decrease of the local maxima was observed.

Conclusion: Wavelet-based methods can increase the SNR without diminishing the signal amplitude, while preserving the spatial resolution of the image. The anatomical localization is strongly improved.

Key Words: functional magnetic resonance imaging; fMRI; general linear model; wavelet analysis; wavelet thresholding
J. Magn. Reson. Imaging 2003;17:20–30.

ALTHOUGH FUNCTIONAL MAGNETIC RESONANCE IMAGING (fMRI) provides excellent images with a high spatial and temporal resolution, it often results in a bad signal-to-noise ratio (SNR) due to biological heterogeneity and scanner-induced noise. To improve the SNR, we present an approach that combines wavelet-based methods with the general linear model.

Max Planck Institute of Cognitive Neuroscience, Leipzig, Germany.
*Address reprint requests to: K.M., Max Planck Institute of Cognitive Neuroscience, Stephanstrasse 1a, D-04103 Leipzig, Germany. E-mail: karstenm@cns.mpg.de
Received February 25, 2002; Accepted September 16, 2002.
DOI 10.1002/jmri.10219
Published online in Wiley InterScience (www.interscience.wiley.com).

Wavelets are widely used in signal and image processing. The most important applications of wavelets are image compression and noise reduction. Wavelets have also been applied in the fMRI context (1–14). Recently, wavelet analysis of fMRI time series was combined with the general linear model (2). In contrast to this approach, our method performs a spatial multidimensional wavelet transform to contrast images.

In standard fMRI data evaluation, a spatial Gaussian filter is applied to the data, which in general leads to an increased SNR. However, the application of spatial Gaussian filters should be considered as problematic because any monoresolution filter reduces the real resolution of the images. This can result in a smeared set of spatial undissociable activations. Moreover, these filters cause a decrease of the signal independent of the spatial structure of the images. In some cases, activation areas may completely disappear.

To improve the SNR and prevent these effects, monoresolution filters should not be used. Different brain regions have to be filtered differently, taking their spatial properties into account. Using the wavelet transform, the multiresolution analysis provides the representation of the signal over several spatial resolution scales. Thus, it is possible to produce almost optimal spatially adaptive filters. Ruttimann et al. (1) developed an approach to derive the optimal adaptive filters by investigating the wavelet coefficients at various resolution levels of the images. Their method was derived from the fact that a spatially localized signal can be represented by a small number of wavelet coefficients, while the power of white noise is uniformly spread throughout the wavelet space.

The method of Ruttimann et al. (1) is based on the statistical evaluation of a number of difference images obtained by means of several on/off blocks. Under the null hypothesis of no effect, these difference images can be assumed to be random fields of identically and independently distributed Gaussian noise. While performing orthonormal linear transformations, the wavelet transform does not change the distribution properties of the difference images. Thus, the null hypotheses can be tested in the wavelet space by comparing each test statistic to the appropriate chi-square quantile. Hereafter, a two-sided z-test is applied to the remaining wavelet coefficients. To adjust for multiple compari-

sons, the Bonferoni correction method is used. The last step of the method is the inverse wavelet transformation.

The results of the method show a rapid improvement of the SNR. This improvement was assessed by Desco et al. (3), who investigated the performance of different wavelet decomposition schemes using realistic computer-simulated phantom data. Additionally, they examined the influence of several types of wavelet basis functions on the size of the activation area and the activity level. No major differences between various wavelet basis families, with the exception of the Gabor wavelet transform, were found. However, their simulation showed that lower wavelet orders and resolution depths should be used to obtain optimal results. In accordance with previous findings (1,4), Desco et al. (3) concluded that multiresolution methods clearly outperform the standard approach because they improve sensitivity and can locate small activation areas. Thus, wavelet-based methods should be preferred over spatial filtering to improve the SNR.

The approach of Ruttimann et al. (1) is limited to images acquired under two experimental conditions using long blocks of stimulation. However, recent neuropsychological studies have used many conditions and more complicated experimental designs with event-related paradigms. Often, very short stimuli have been used. Therefore, the aim of this work is to present a generalization of Ruttimann's method combining wavelet-based methods with the general linear model. A detailed treatment of the general linear model can be found in Refs. 15–17.

The key idea is to consider the effect values (so-called betas in the general linear model) using wavelet analysis. Even if the signal is highly correlated, the correlation between the wavelet coefficients will be small (5). Thus, under the null hypothesis of no effect, the wavelet coefficients of contrast images (which are linear combinations of betas) can be assumed to be independently and identically distributed, and Gaussian. Using an improved variance estimate obtained from pooling the residual variances over all intracranial voxels, whole wavelet space partitions as well as single wavelet coefficients can be statistically assessed.

To demonstrate the approach, we apply the method to fMRI data acquired in a recent study by Zysset et al. (18). Those data were obtained using a variation of the Stroop task, which is called "color-word matching Stroop." For comparison, we perform a standard fMRI data evaluation, presmoothing the images by applying a spatial Gaussian filter.

MATERIALS AND METHODS

Wavelet Decomposition

In the following, a brief introduction to wavelet decomposition is given, describing the basic relations that are used in this context. For a detailed treatment, see the monograph of Daubechies (19). Bultheel (20) gave an excellent introduction to wavelet theory and multiresolution analysis.

Let us consider decompositions of a signal f into basis functions of the space of square integrable functions L_2 on the real axis $\mathbf{R}$. The x-axis can coincide with the temporal domain, if f is a time course. However, in our case we will investigate the wavelet transform for images, i.e., the x-axis will coincide with the spatial domain.

A signal is said to be local if it has almost compact support, i.e., if most of its energy is located in a finite interval. If δ denotes the Dirac delta function, then the functions $\{\delta(x - u)\}_{u\in\mathbf{R}}$ are a set of orthonormal basis functions in L_2. Those basis functions are extremely local in the spatial domain, but in the frequency domain the Fourier transform of $\delta(x - u)$ is supported on the whole real axis.

In a different situation, one might consider the orthonormal basis $\{e^{iux}\}_{u\in\mathbf{R}}$. Now, the basis functions are associated with just one frequency, and in the spatial domain they are supported on the whole axis.

Thus, wavelets are basis functions that are local in the spatial and frequency domain.[1] This property makes wavelets very suitable for analyzing a signal by decomposing it into components that are local in both domains. We can look at the signal in local regions of the image using a window moving over the signal. At the same time, we can consider several resolutions that would correspond to a sliding window over all possible frequencies.

If they are still an orthonormal set, wavelets become particularly interesting because of their decorrelating property. After a wavelet transformation, the noise is uniformly spread throughout the wavelet space, whereas the noiseless signal is effectively compressed into a small number of coefficients (this is also called the whitening property (5). Thresholding the smaller uncorrelated coefficients removes noise. Thus, wavelet denoising techniques can be considered to be a nonparametric method. No particular model or parameters must be specified a priori.

In the remainder of this section a brief introduction is given to the computation of the wavelet transforms. Orthonormal wavelet bases can be constructed via a given scaling function $\phi(x)$ and its associated mother wavelet

$$\psi(x) = \sum_k g(k)\phi(2x - k) \tag{1}$$

using a suitable weighting sequence $g(k)$. The scaling function $\phi(x)$ is determined by a so-called refinement filter $h(k)$ and a certain dilation equation:

$$\phi(x) = \sum_k h(k)\phi(2x - k). \tag{2}$$

This is also called a two-scale relation. If that dilation equation (Eq. [2]) can be solved for some choice of the refinement filter $h(k)$, the functions

$$\phi_{jk}(x) = 2^{j/2}\phi(2^j x - k) \tag{3}$$

[1]Considering the Fourier-Heisenberg uncertainty principle, it is not possible to have compactness in both the spatial and the frequency domain.

may be considered. The functions ϕ_{jk} are often called "father functions" or "father wavelets." The weighting sequence $g(k)$ and the refinement filter $h(k)$ can be selected such that the functions

$$\psi_{jk}(x) = 2^{j/2}\psi(2^j x - k) \tag{4}$$

form an orthonormal basis of L_2. Using the inner product in L_2, the functions $\{\psi_{jk}\}$ form an orthonormal set, if

$$\langle \psi_{jk}, \psi_{lm} \rangle = \delta_{jl}\delta_{km}. \tag{5}$$

The translations k of the wavelet correspond to a sliding window in the spatial domain. The dyadic dilations j of the wavelet will have a windowing in the frequency domain (20). Thus, using the wavelet transform, one can produce spatially adaptive filters. In contrast to monoresolution filters, spatially adaptive filters can handle different regions of an image with different filter widths, which can be derived considering the signal in various resolution levels.

The wavelet and the approximation coefficients have the form

$$d_j(k) = \langle f, \psi_{jk} \rangle \quad \text{and} \quad c_j(k) = \langle f, \phi_{jk} \rangle, \tag{6}$$

respectively. The set of coefficients $d_j(k)$ is called the wavelet transform of the signal f with respect to the basis $\{\psi_{jk}\}$.

In practice, the function f is a sampled signal, i.e., f is discrete. Then the wavelet decomposition can be performed only over a finite number of resolution levels J. The signal f can be represented in the form

$$f(x) = \sum_{j=1}^{J} \sum_{k} d_j(k)\psi_{jk} + \sum_{k} c_J(k)\phi_{Jk} \tag{7}$$

The wavelet transform (Eq. [6]) can be easily extended to the multidimensional case by applying the wavelet transform successively along the separate dimensions of the data (1,20,21). Thus, the wavelet transform in two dimensions can be computed applying the one-dimensional transform successively along the columns and the rows of the image (21). Therefore, the two-dimensional wavelet transform generates four quadrants at each resolution. In the q-dimensional case, 2^q different types of basis functions are generated, i.e., 2^q quadrants are generated at each resolution level. Let $\mathbf{x} = (x_1, \ldots, x_q)$. Then, the q-dimensional scaling functions are

$$\phi_{j\mathbf{k}}(\mathbf{x}) = \prod_i \phi_{j,k_i}(x_i) \tag{8}$$

where $\mathbf{k} = (k_1, \ldots, k_q)$ is a q-dimensional vector of indices. The q-dimensional wavelet functions can be obtained in the same way by replacing one or several factors in Eq. [8] by a wavelet function ψ_{j,k_i} (see Eq. [4]). According to the notation of Ref. 1, let $b_1, \ldots, b_q$ be a binary vector that indicates the replacement of the factors in Eq. [8], i.e., b_i is set to one if ϕ_{j,k_i} is replaced by ψ_{j,k_i}. If the resulting factors are denoted by φ_{j,k_i}, the q-dimensional wavelet functions are

$$\omega^m_{j\mathbf{k}}(\mathbf{x}) = \prod_i \varphi_{j,k_i}(x_i), \quad m = \sum_i b_i 2^{i-1}. \tag{9}$$

The index $m = 1, \ldots, 2^q - 1$ is the so-called spatial direction indicator. For example, in the 2-dimensional case, the directions $m = 1, 2, 3$ correspond to wavelets that are oriented along the vertical, horizontal, and diagonal directions, respectively. Using Eq. [9], the multidimensional wavelet and approximation coefficients have the form

$$d^m_j(\mathbf{k}) = \langle f, \omega^m_{j\mathbf{k}} \rangle \quad \text{and} \quad c_j(\mathbf{k}) = \langle f, \phi_{j\mathbf{k}} \rangle, \tag{10}$$

respectively. For a more detailed treatment of the theory, we refer to the original paper (21). Also see Ref. 22 for practical implementation.

Wavelet Thresholding

As noted in the previous section, noise is uniformly spread throughout the wavelet space, whereas the noiseless signal is effectively compressed into a small number of coefficients (23). Therefore, thresholding the smaller uncorrelated coefficients removes noise.

Thresholding policies for wavelet filtering were developed by Donoho and Johnstone (23,24). They proposed a so-called universal threshold

$$\Theta = \hat{\sigma}\sqrt{2 \log N} \tag{11}$$

that is based on the estimated noise variance $\hat{\sigma}$. The idea is to remove all wavelet coefficients that are smaller than the expected coefficients of an assumed noise, where N is the number of measurements. There are two standard thresholding choices: hard thresholding

$$\hat{d}_{j;H}(k) = d_j(k)I(|d_j(k)| > \Theta) \tag{12}$$

and soft thresholding

$$\hat{d}_{j;S}(k) = \mathrm{sgn}(d_j(k))(|d_j(k)| - \Theta)I(|d_j(k)| > \Theta) \tag{13}$$

where $I(A)$ is the indicator function that yields one, if condition A is fulfilled, and zero otherwise. Hard thresholding is an unbiased procedure that does not change the size of the preserved wavelet coefficients. This can lead to noisy artifacts because of the hard separation of noise and signal. Soft thresholding reduces the value of the preserved coefficients. However, this leads to an increased bias, because the preserved coefficients are reduced by an equal amount (see Refs. 23 and 24). Ruttimann et al. (1) introduced a thresholding concept from the statistical point of view. Because insignificant wavelet coefficients are set to zero, this concept is a type of hard thresholding. Our approach is an enhancement of Ruttimann et al.'s method, whereby the general linear model is used to obtain appropriate thresholds.

Statistical Analysis

In this section we describe a wavelet-based detection method for contrast images obtained by the general linear model. The wavelet statistics are based on a two-stage approach of Ruttimann et al. (1) that tests for significant wavelet coefficients in several resolution channels.

The general linear model is often used for evaluation of fMRI data. It is implemented in several software packages. An introduction to the general linear model with respect to experimental designs can be found in Ref. 16. The general linear model has the form

$$\mathbf{Y} = \mathbf{X}\beta + \mathbf{e} \tag{14}$$

where $\mathbf{Y}$ is the response variable of unsmoothed data for each observation. In most cases, the response variable is a matrix of all time-series of all voxels. We will assume that the components of the error term $\mathbf{e}$ are independently and normally distributed with mean 0 and variance σ^2. The design matrix $\mathbf{X}$ is the so-called predictor variable and contains the covariates of the model. The number of covariates coincides with the number of columns of $\mathbf{X}$.

Because of the unknown autocorrelation of the observed data, $\mathbf{Y}$ is multiplied by a convolution matrix $\mathbf{K}$ whose rows represent the hemodynamic response function (16). To obtain an estimate of β, the least-squares estimation to the smoothed observations yields

$$\mathbf{b} = \mathbf{G}^{+}\mathbf{K}\mathbf{Y} \tag{15}$$

where

$$\mathbf{G}^{+} = (\mathbf{G}^{\mathrm{T}}\mathbf{G})^{-1}\mathbf{G}^{\mathrm{T}} \tag{16}$$

is the so-called Moore-Penrose inverse of $\mathbf{G}$, and $\mathbf{G} = \mathbf{K}\mathbf{X}$ denotes the convolved design matrix $\mathbf{X}$. Using the estimated parameters (Eq. [15]), statistical inferences about effects of interest can be addressed using linear compounds or contrasts. A contrast vector $\mathbf{c}$ is a set of weights that sum to zero. A contrast is a linear combination of parameter estimates

$$\mathbf{f} = \mathbf{c}\mathbf{b} \tag{17}$$

using a contrast vector $\mathbf{c}$. If there is only one effect, the contrast vector is simply $\mathbf{c} = 1$. Often, $\mathbf{f}$ is called an estimation of the signal. The variance-covariance matrix of the parameter estimates can be expressed as

$$\mathrm{Var}(\mathbf{b}) = \sigma^2\mathbf{G}^{+}\mathbf{V}(\mathbf{G}^{+})^{\mathrm{T}} \tag{18}$$

where $\mathbf{V} = \mathbf{K}\mathbf{K}^{\mathrm{T}}$ represents the assumed autocorrelation (25). An unbiased estimator for the variance σ^2 in Eq. [18] can be obtained by dividing the residual sum of squares by its expectation in the following way:

$$\hat{\sigma}^2 = \frac{\mathbf{r}^{\mathrm{T}}\mathbf{r}}{\mathrm{tr}(\mathbf{R}\mathbf{V})} \tag{19}$$

where $\mathbf{r} = \mathbf{R}\mathbf{K}\mathbf{Y}$ is the vector of residuals (16) and $\mathbf{R} = \mathbf{I} - \mathbf{G}\mathbf{G}^{+}$ is the pre-residual matrix (see Ref. 25). The estimated variance associated with the contrast $\mathbf{f}$ can be obtained by

$$\begin{aligned}\hat{\sigma}_{\mathbf{f}}^2 &= \mathrm{Var}(\mathbf{f}) = \mathrm{Var}(\mathbf{c}\mathbf{b})\\ &= \mathbf{c}\ \mathrm{Var}(\mathbf{b})\mathbf{c}^{\mathrm{T}}\\ &= \sigma^2\mathbf{c}\mathbf{G}^{+}\mathbf{V}(\mathbf{c}\mathbf{G}^{+})^{\mathrm{T}}.\end{aligned} \tag{20}$$

Because the error term $\mathbf{e}$ is homogeneous by assumption, an improved variance can be estimated by pooling $\hat{\sigma}_{\mathbf{f}}^2$ over all intracranial voxels. Let $\mathcal{I}$ be the set of all intracranial voxels, N be the number of elements of $\mathcal{I}$, and $\hat{\sigma}_{\mathbf{f}}^2(\mathbf{k})$ denote the estimated variance of voxel $\mathbf{k}$. Then

$$\hat{\Sigma}_{\mathbf{f}} = \frac{1}{N}\sum_{\mathbf{k}\in\mathcal{I}}\hat{\sigma}_{\mathbf{f}}^2(\mathbf{k}). \tag{21}$$

This improved variance $\hat{\Sigma}_{\mathbf{f}}$ yields an approximation of the variance of the error term $\mathbf{c}\mathbf{e}$ (26).

In order to detect significant activations, contrast images are investigated using methods of multiresolution analysis. This approach is based on wavelet thresholding and Bonferoni correction. The most important property of the discrete wavelet transform is the following: Generally the correlation between the wavelet coefficients of a signal will be small even if the signal is highly autocorrelated itself. The errors in the wavelet domain can be assumed to be independently and identically distributed, and Gaussian. Furthermore, under the null hypothesis, the scaled sum of squares of any set of coefficients follows the chi-square distribution. In conjunction with the orthogonality of the wavelet decomposition, these properties permit the two-stage approach of statistical postprocessing developed by Ruttimann et al. (1).

The first stage of the procedure considers the question of whether there is enough power in the resolution channels. For this purpose, the contrast values (Eq. [17]) are transformed into the wavelet domain in order to perform a multiresolution decomposition. At each resolution level j, the wavelet coefficients of $\mathbf{f}(\mathbf{k})$ are denoted by $d_j^m(\mathbf{k})$, where m denotes the three spatial directions in each resolution level. See Eqs. [9] and [10] for the computation of the coefficients $d_j^m(\mathbf{k})$.

Let the wavelet coefficients be normalized by dividing by the improved variance (Eq. [21]) as follows:

$$\tilde{d}_j^m(\mathbf{k}) = \frac{d_j^m(\mathbf{k})}{\hat{\Sigma}_{\mathbf{f}}}. \tag{22}$$

Under the null hypothesis and the assumption of a homogeneous error term $\mathbf{e}$, the normalized wavelet coefficients $\tilde{d}_j^m(\mathbf{k})$ follow the standard Gaussian distribution $\mathcal{N}_{0,1}$. Furthermore,

$$\tilde{d}_j^m(\mathbf{k})^2 \sim \text{iid } \chi_1^2. \tag{23}$$

Based on Eq. [23], the sum of the squared normalized wavelet coefficients is a chi-square variate where the degree of freedom coincides with the number of summation terms. This leads to a test procedure of the statistical significance of the wavelet coefficients of each resolution level j. Let I denote the indicator function. Then, the null hypothesis of no activation is tested using

$$\check{d}_j^m(\mathbf{k}) = \tilde{d}_j^m(\mathbf{k}) I\left(\sum_{\mathbf{k}\in\mathcal{I}_{j,m}} \tilde{d}_j^m(\mathbf{k})^2 > \Theta_j\right) \tag{24}$$

and

$$\Theta_j = \hat{\Sigma}_{\mathbf{f}} \chi^2_{k_{j,m};\alpha} \tag{25}$$

where $k_{j,m}$ is the number of intracranial wavelet coefficients $\mathbf{k} \in \mathcal{I}_{j,m}$ at level j and directions m. The significance level

$$\alpha = p/3J \tag{26}$$

is adjusted using the Bonferoni correction method, where J denotes the number of statistical tests that coincides with the number of detail levels. Nonsignificant wavelet coefficients are assumed to provide only noise. They are therefore excluded from further analysis.

The next step of the method is based on the standard Gaussian distribution of the normalized wavelet coefficients. Thus, the null hypothesis of no activation is tested by comparing each wavelet coefficient with the standard Gaussian quantile

$$\check{d}_j^m(\mathbf{k}) = \tilde{d}_j^m(\mathbf{k}) I(|\tilde{d}_j^m(\mathbf{k})| > \tau) \tag{27}$$

where

$$\tau = \hat{\Sigma}_{\mathbf{f}} z_{\alpha_1}. \tag{28}$$

This corresponds to a two-sided z-test for the wavelet coefficients of the channels (resolution levels j and directions m) that were determined to carry significant power. The number of statistical tests coincides with the number of wavelet coefficients in the significant channels.

To take into account the false-positive detection rate, the significance level is controlled by a Bonferoni correction to adjust for multiple comparisons. The significance level α_1 can be adjusted by

$$\alpha_1 = \frac{p}{\sum_{j,m\in\mathcal{I}_{j,m}} k_{j,m}} \tag{29}$$

where $\mathcal{I}_{j,m}$ is the set of remaining intracranial wavelet coefficients in the resolution level j and direction m. In the wavelet domain, a Bonferoni correction is not too conservative because of the decorrelating property of the wavelet transform. The Bonferoni correction is optimal, if the hypotheses being tested are independent of each other (27). The method is also certainly valid for the detection of the false positives. Because of the independence of the wavelet coefficients and the unknown smoothness, the method of Worsley et al. (26) is not applicable in this context.

Hence, the final step of the procedure is to compute the inverse discrete wavelet transform to the threshold wavelet coefficients.

Stimuli and Imaging Procedure

We applied wavelet-based methods to fMRI data acquired in a previous study by use of the Stroop interference task (18).

In the present study, the data from two subjects (22 and 23 years old) were used. Both subjects were native German speakers; they were right-handed and had normal or corrected-to-normal vision, and normal color vision. The subjects provided informed consent prior to the scanning session. Stimuli were projected by an LCD projector onto a back-projection screen mounted in the bore of the magnet behind the subject's head. Subjects viewed the screen wearing mirror glasses, which were equipped with corrective lenses as necessary.

The subjects were told that they would see two rows of letters, and were instructed to decide whether the color of the top-row letters corresponded to the color name written in the bottom row. During the neutral trials, the letters in the top row were "XXXX" printed in red, green, blue, or yellow, and the bottom row consisted of the words "RED," "GREEN," "BLUE," and "YELLOW" printed in black. For the congruent trials, the top row consisted of the words "RED," "GREEN," "BLUE," and "YELLOW" printed in the congruent color. The incongruent trial was identical to the congruent one except that the color word in the top row was printed in an incongruent color, e.g., "GREEN" printed in red.

For each session, stimulation started and ended with a black screen for 30 seconds containing the fixation on a small gray dot. For the Stroop task paradigm, four neutral blocks alternated with four congruent and four incongruent blocks. If no response was given after a maximal time of 1.5 seconds, the next trial was presented. In the case of a response, the stimulus disappeared and the residual time was filled by a blank screen. Given a fixed interstimulus interval of 1.5 seconds, the subjects completed 20 trials during each (neutral/congruent/incongruent) block of 30 seconds, 80 trials of each type during a single session, and 160 trials during both sessions.

Imaging was performed at 3T on a Bruker Medspec 30/100 system, and the standard birdcage head coil was used. The subjects lay on the scanner bed and cushions were used to reduce head motion. In addition to the functional data sets, high-resolution whole-brain images were recorded to improve the localization of activation foci using a T1-weighted 3D segmented Modified Driven-Equilibrium Fourier Transform (MDEFT) sequence (128 slices sagittal, 1.5 mm thickness, 256 × 256 pixel matrix). For details see Ugurbil et al. (28) and Lee et al. (29).

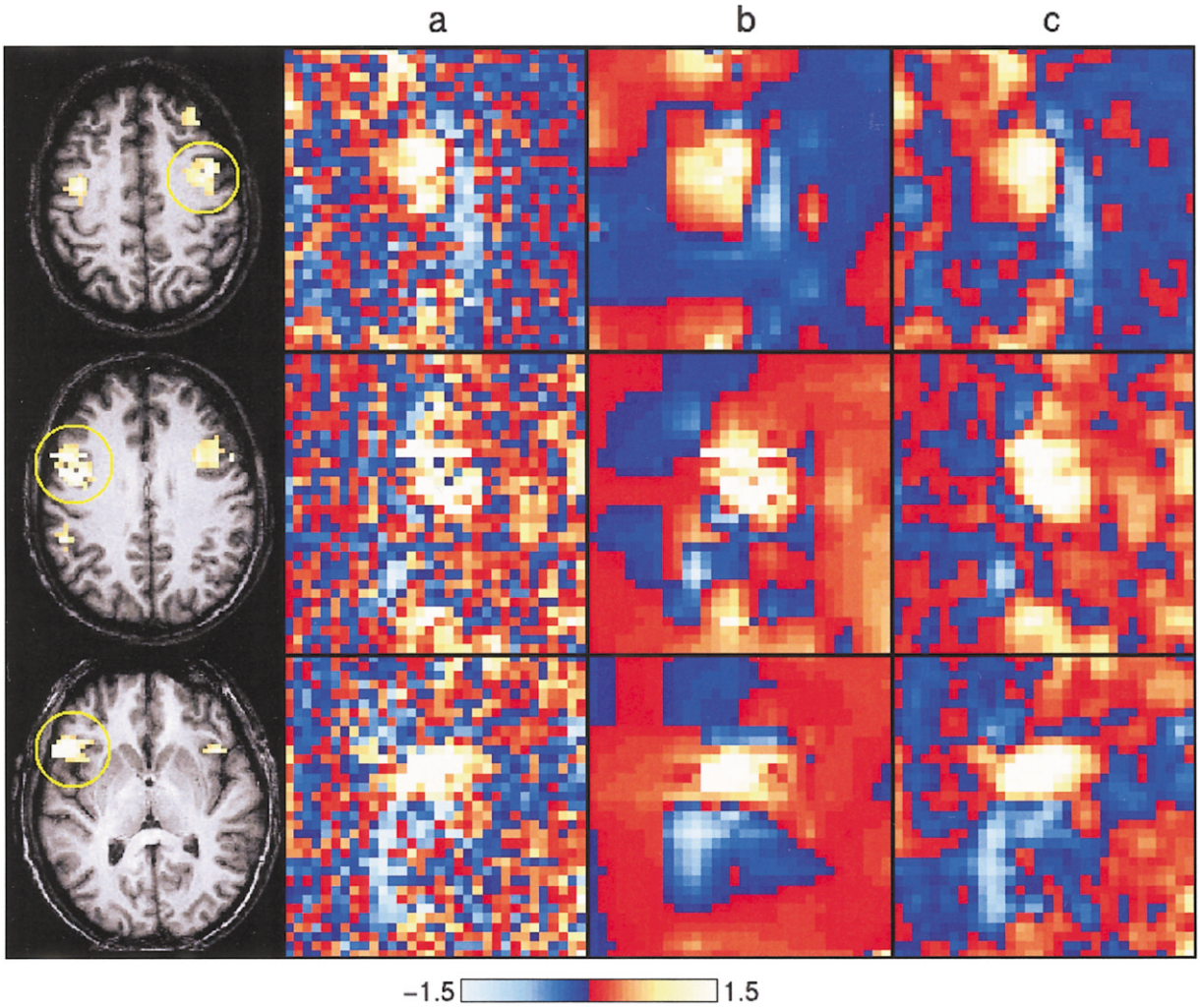

Figure 1. Several axial slices and zoomed contrast images of the subject HS obtained (**a**) without any spatial filtering, (**b**) using the wavelet-based approach, and (**c**) applying a spatial Gaussian filter. Both the wavelet and the Gaussian filter lead to reduced noise. However, the wavelet-based method depends on the variance of the signal (see Eq. [21]), and therefore leads to a stronger improvement of the SNR compared with Gaussian filtering (see Table 1).

To align the echo-planar images to the 3D images, conventional anatomical images in plane with the functional images were acquired as an intermediate step using a T1-weighted MDEFT (28) sequence (TE = 10 msec, TR = 1300 msec, 256 × 256 matrix). These images were obtained with a non-slice-selective inversion pulse followed by a single excitation of each slice (30).

Finally, 16 functional slices (192 mm FOV, 64 × 64 pixel matrix, 5-mm slice thickness, 2 mm interslice distance) were acquired parallel to the AC-PC plane covering the whole brain. Functional images were acquired using a single-shot gradient-recalled echo-planar imaging (EPI) sequence (TR = 2000 msec, TE = 30 msec, 90° flip angle). Two functional sessions with 210 scans each were recorded for all subjects.

Data Analysis

The fMRI data were processed on an SGI Origin 2000 using software developed at the Max Planck Institute of Cognitive Neuroscience in Leipzig, Germany. Preprocessing, registration, and visualization of the data were performed using the software package Lipsia (31). The tool for the wavelet-based procedure was implemented as explained in the Statistical Analysis section.

Functional data were corrected for motion using a matching metric (rigid-body realignment) based on linear correlation. To correct for the temporal offset between the slices acquired in a session, a sinc-interpolation based on the Nyquist-Shannon theorem was applied. The mathematical basis is the well-known Nyquist-Shannon sampling theorem. Any continuous band-limited function is completely determined by discrete measurements taken at a constant sampling interval. In other words, any function value for which no direct measurement exists can be reconstructed exactly and without loss of information by interpolating between the measurement points (22,32).

Temporal filtering was done applying a high-pass filter for both sessions with a cutoff frequency of 1/120 Hz. Filtering was performed by multiplying the signal after Fourier transformation by a sigmoidal cutoff function and converting it back by the inverse Fourier trans-

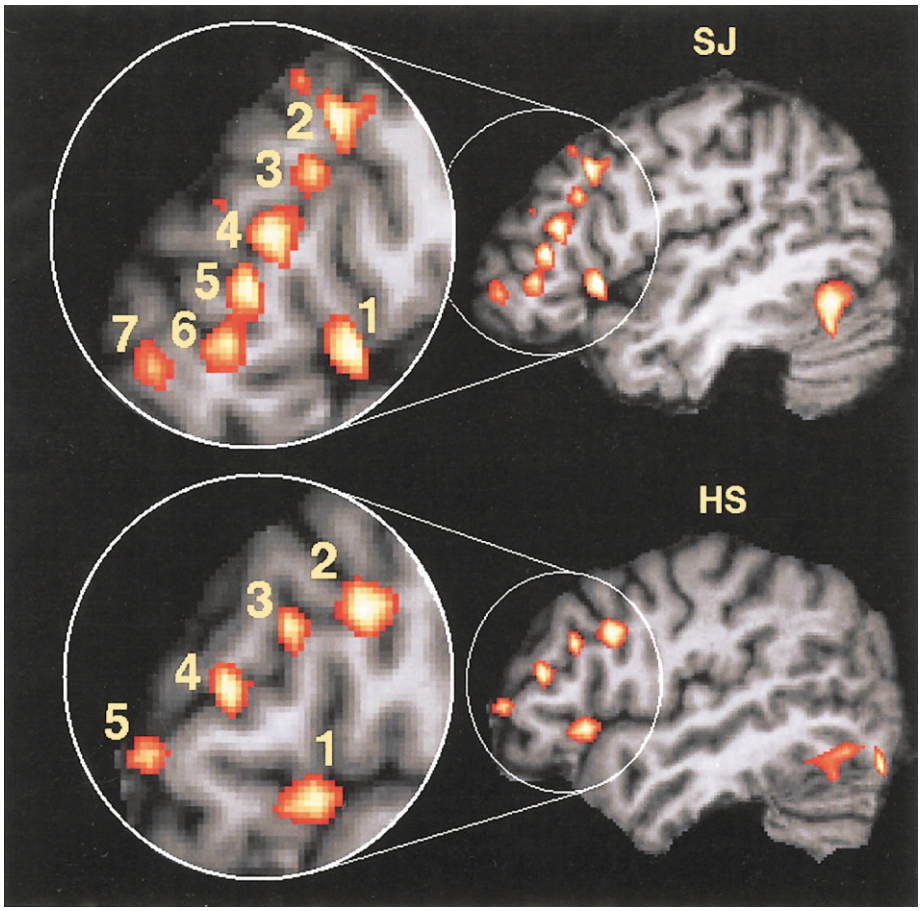

Figure 2. Sagittal slices (left lateral, X = −44 and X = −46, respectively) of two individual subjects, showing a chain of dissociable activations obtained by the wavelet-based approach using a *P*-level of 0.05. The activation IDs correspond to the numbering of Table 2. For corresponding axial slices and the color map, see Figures 3 and 4.

form. The effect of such a transformation is a baseline correction of the signal (see Ref. 31).

To compare the effect of the wavelet-based filtering with a standard fMRI data analysis, three analyses were performed. In the first analysis, no spatial filter was applied. In the second analysis, a spatial two-dimensional Gaussian filter with a standard deviation (SD) of 0.8 was applied to each fMRI slice. With respect to the voxel size, the SD of 0.8 leads to a kernel size of 5.65 mm. The data were analyzed a third time using the wavelet-based approach described herein.

The statistical evaluation was based on a least-squares estimation using the general linear model for serially autocorrelated observations (15–17). The design matrix was generated using all four experimental conditions (blank screen/neutral/congruent/incongruent). Thus, the design matrix consists of four columns that were generated using a boxcar function. The model equation, including the observation data, the design matrix, and the error term were convolved with a Gaussian kernel (Eq. [15]). The Gaussian kernel of 4 seconds FWHM was chosen to emulate the dispersion associated with the hemodynamic response function (15,16). Combining the parameter estimates for the neutral and incongruent condition, contrast and variance images were generated as described in Eqs. [17] and [20]. Note that the other conditions also served as covariates in the design matrix. Thus, all conditions were used for parameter estimation. Using the variance images, an improved variance was estimated as in Eq. [21].

To detect significant activations, wavelet-based methods were applied to contrast images. As the wavelet basis, the Daubechies wavelets (19) were chosen. We also tried other wavelet basis families but found no major differences. Using synthetic data, Desco et al. (3) investigated the influence of the choice of the wavelet basis. They also found no major differences. However, in their study, the Gabor decomposition yielded the best results. The simulation (3) showed that lower wavelet orders and resolution depths should be used to obtain optimal results. Therefore, the number of four coefficients was chosen.

After computing the discrete wavelet transform to the contrast values, a two-stage thresholding procedure (1) was applied to the wavelet coefficients. For each of the resolution levels and each of the three directions, the null hypothesis of no activation was tested by comparing each test statistic to the appropriate chi-square quantile (see Eqs. [24] and [25]). Nonsignificant coefficients were excluded from further analysis. The remaining coefficients were used to compute a second test of statistics by dividing each wavelet coefficient by the estimated noise variance (Eq. [22]). Then the null hypothesis of no activation was tested by comparison of each test statistic to the appropriate standard Gaussian quantile (Eq. [27]). The Bonferoni method was used

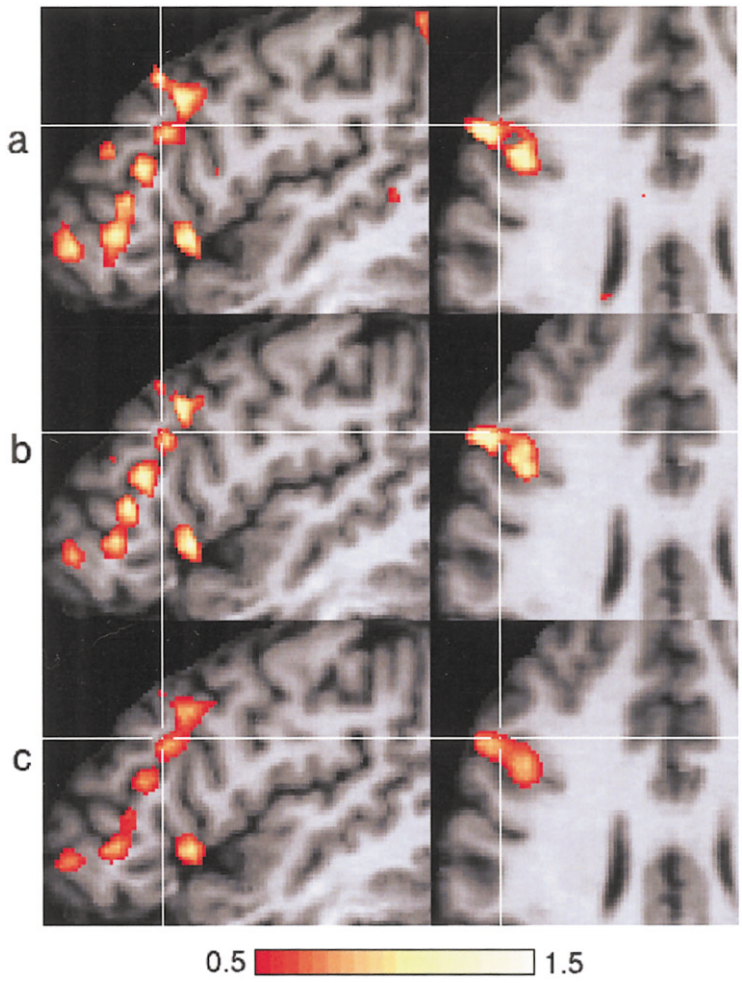

Figure 3. Axial and sagittal slices (X = −44, Z = 26) of the subject SJ through the left lateral prefrontal cortex. The figure shows contrast images obtained **(a)** without any spatial filtering, (first row) **(b)** using the wavelet-based approach, (second row) and **(c)** applying a spatial Gaussian filter (last row). The local maxima of the activations are listed in Table 2. See Fig. 2 for allocating the activations to the IDs of Table 2. Using the wavelet filter **(b)**, the SNR increased, and activations were even more dissociable than in the original unfiltered data. In contrast, the application of the Gaussian filter **(c)** leads to reduced contrast values in all activations.

at both stages to adjust the results for multiple comparisons (see Eqs. [26] and [29]).

To align the contrast images with a 3D stereotactic coordinate reference system, a rigid linear registration with six degrees of freedom (three rotational and three translational) was performed. The rotational and translational parameters were acquired on the basis of the MDEFT slices to achieve an optimal match between these slices and the individual 3D reference data set. This 3D reference data set was acquired for each subject during a prior scanning session. The MDEFT volume data set with 160 slices and 1 mm slice thickness was standardized to the Talairach stereotactic space (33). The resulting parameters were then used to transform the contrast images using trilinear interpolation, so that the resulting images were aligned with the stereotactic coordinate system.

For the contrast images, local maxima were computed. A pixel was defined to be a local maximum if its value exceeded 0.5 and if it was largest within a 5 mm radius. Local maxima residing in activation areas smaller than 50 mm^2 were not reported.

RESULTS

For the color-word matching Stroop task, the main contrast was the incongruent condition against the neutral condition. This interference condition elicited activations in the lateral prefrontal cortex in the form of a chain of activations along the left inferior frontal sulcus (IFS). These activations were located from the anterior tip of the IFS (BA 46/9) through the middle IFS up to the junction point of the posterior IFS and the precentral sulcus (BA 6). Figure 2 shows a strong activation in the inferior frontal gyrus (BA 44). These results were also reported by Zysset et al. (18).

Figures 1, 3, and 4 compare the multiresolution methods with the application of a monoresolution filter, showing contrast images for (a) without any spatial filtering, (b) with the wavelet-based postprocessing using a *P*-level of 0.05, and (c) with a spatial Gaussian monoresolution filter of 5.65 mm FWHM. Table 1 shows the variance for thermal and other system noise determined in appropriate regions of interest (ROIs) outside the brain. Both the wavelet and the Gaussian filter lead to reduced noise (see Fig. 1). However, the application of a monoresolution filter leads to reduced effect values in the contrast images, as shown Figures 3c and 4c. When a Gaussian filter was applied to the data, all local maxima of the contrast images were considerably lower than in the results without spatial smoothing. On average, the signal height was only 60% of the original signal (see last column of Table 2). Thus, when higher thresholds were selected for the activation maps, sev-

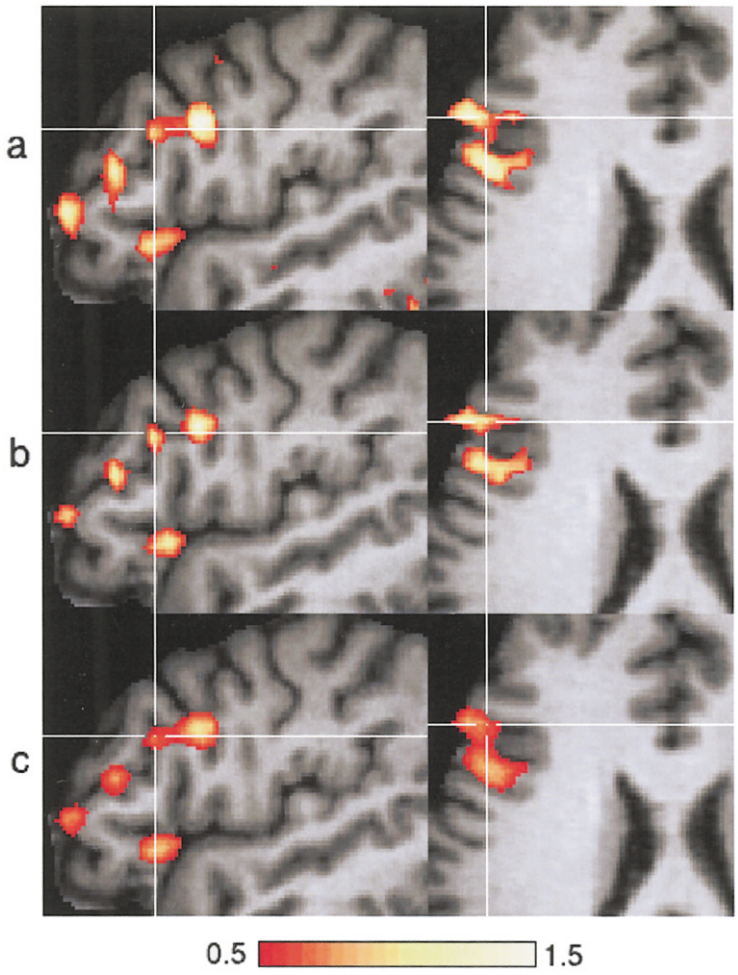

Figure 4. Axial and sagittal slices (X = −46, Z = 23) of the subject HS. See Fig. 3 for details.

eral activations vanished completely. Furthermore, the monoresolution filter also reduced the real resolution of the activation maps. The activations along the IFS were larger and no longer dissociable. They could be inadvertently interpreted as a single large activation around the IFS, as shown in Figures 3c and 4c.

In contrast to the Gaussian filter, the application of the wavelet-based method increased the SNR without the unwanted effects described above. Figures 3b and 4b show a set of clearly distinguishable activations along the IFS. Because of the noise reduction, the activations were even more dissociable than in the original unfiltered data (compared with Figs. 3a and 4a; see also Fig. 1). Furthermore, there was no significant decrease of the maxima of the contrast images. Using the wavelet-based filtering, the size of the effect values was (on average) more than 90% of the original values (see Table 2).

Table 1
Thermal and Other System Noise With Different ROI Size*

Subject	N_0	$\sigma_0^2 \times 10^3$	$\sigma_{0w}^2 \times 10^3$	$\sigma_{0g}^2 \times 10^3$
SJ	2496	21.76	1.19 (5.47)	5.38 (24.72)
	3264	21.45	1.33 (6.20)	5.22 (24.34)
	4032	21.72	1.45 (6.68)	5.25 (24.17)
HS	2496	26.90	2.43 (9.03)	6.70 (24.91)
	3264	25.85	2.42 (9.36)	6.28 (24.29)
	4032	26.26	2.42 (9.22)	6.17 (23.50)

*Raw noise variance σ_0^2 determined in several ROIs with different size N_0. The column σ_{0w}^2 shows the reduction of the noise variance using wavelet filtering with $P = 0.05$, and the last column σ_{0g}^2 shows the reduction of the noise variance using Gaussian filtering with 5.65 mm FWHM. The bracketed numbers express the noise decrease in percent. Using the Gaussian filter, the noise decrement only depends on the selection of the filter width. In contrast, the result of wavelet-based noise reduction depends on the variance of the signal (see Eq. [21]).

DISCUSSION

The general idea of our approach is to combine wavelet-based methods with the general linear model. Estimating the variance-covariance matrix of the model and computing the spatial wavelet transform of contrast images, wavelet coefficients can be statistically assessed in a postprocessing step. This removes noise and leads to an increased SNR.

Recent works by Ruttimann et al. (1) and Brammer (4) presented a multiresolution approach for fMRI data. They reported a higher sensitivity in the detection of activated brain areas compared to more established methods. However, their method is restricted to the investigation of differences between images acquired under two experimental conditions using long blocks of

Table 2
Local Maxima Residing in Activation Areas of Contrast Images*

Subject	ID	x	y	z	c_{orig}	c_w	c_g
SJ	1	−50	11	−1	3.53	3.41 (96.6)	1.87 (53.0)
	2	−38	10	29	1.30	1.28 (98.4)	0.89 (68.5)
	3	−48	18	26	1.63	1.47 (90.2)	0.97 (59.5)
	4	−44	24	16	1.13	1.21 (107.1)	0.77 (68.1)
	5	−48	28	8	1.25	1.23 (98.4)	0.72 (57.5)
	6	−44	31	0	1.22	0.99 (81.1)	0.82 (67.2)
	7	−41	47	−5	1.22	1.13 (92.6)	0.88 (72.1)
HS	1	−55	18	−4	2.38	2.09 (87.8)	1.53 (64.3)
	2	−47	11	26	1.71	1.47 (86.0)	1.22 (71.3)
	3	−52	22	23	1.53	1.29 (84.3)	0.96 (62.7)
	4	−49	32	13	1.31	1.32 (100.8)	0.89 (67.9)
	5	−46	42	4	1.27	1.05 (82.7)	0.89 (70.1)

*The table shows local maxima of activation areas of the left lateral prefrontal cortex. The values c_{orig} are local maxima of contrast images without any spatial filtering, c_w with the wavelet-based postprocessing using a P-level of 0.05, and c_g using a spatial Gaussian monoresolution filter of 5.65 mm FWHM. The bracketed numbers express the signal decrease in percent. The indicated activation IDs correspond to Figure 2.

stimulation. The work of Ruttimann et al. (1) was improved by Feilner et al. (8,9). Under two experimental conditions, a *t*-test can be performed completely in the wavelet domain. Taking into account the variability of each wavelet coefficient separately, their approach works also in the case of nonstationary Gaussian noise. However, their method is still restricted to the standard block paradigm. Many neuropsychological questions require more than two conditions and the ability to handle event-related designs. Therefore, the approach of Ruttimann et al. (1) was enhanced using the general linear model (15,16). Thus, there is no constraint that requires long blocks of stimulation. This strategy allows the treatment of event-related hemodynamic responses evoked by different sorts of stimuli (17). Moreover, single trials may be evaluated.

Although the parameter estimation is performed in the temporal domain, the significance of the coefficients is completely assessed in the wavelet space. Because of the decorrelation property of the wavelet transform, the false-positive rate can be controlled adjusting the significance level using the Bonferoni correction method. The Bonferoni correction is optimal for nearly independent observations (27). Thus, in the wavelet space, Bonferoni correction is a simple type of alpha adjustment that yields optimal results. Random field methods (26) are not applicable to multiresolution approaches because of the independence of the wavelet coefficients and the unknown smoothness (1).

From a practical point of view, our method is easy to integrate into fMRI data processing, because the general linear model is well established for statistical evaluation. Thus, the method can be quickly incorporated into common fMRI software (see, e.g., Refs. 15, 31, and 34). Wavelet thresholding can be easily performed on contrast images after parameter estimation for the model. Once the residual variance is estimated, the wavelet coefficients can be statistically assessed using the chi-square and the standard Gaussian distribution. The resulting maps show a clear improvement of the SNR without destroying the signal, and without decrement of the resolution of the image. Because of the improved SNR, the resulting activations are even more dissociable than in the unfiltered data. The size of the activations does not grow, and the height of the signal does not change significantly.

In standard fMRI data evaluation, the SNR is improved by applying a Gaussian monoresolution filter. The wavelet-based approach was compared with a Gaussian filter with an SD of 0.8 that corresponds to a filter size of 5.65 mm FWHM. This relatively small filter size was chosen to obtain a fair comparison. Some studies have recommended presmoothing the images with a Gaussian filter of 8–12 mm FWHM (15,16). Indeed, the application of a Gaussian filter with such a large filter width can strongly increase the SNR. However, applying a monoresolution filter reduces the real resolution of the image. The image is blurred and some activations are no longer dissociable. This effect can also be observed for relatively small filter widths. With the use of a larger filter, the activations are more undifferentiated, and the anatomical localization is more imprecise. Furthermore, the application of a Gaussian filter destroys the signal. Small activations may vanish completely.

In fMRI group studies, individual brains are often transformed by linear scaling to a standard size (33). However, linear scaling does not consider the anatomical structure of the different brains. Therefore, Gaussian filtering is often used in group studies, because a monoresolution filter reduces the individual specifics in the functional data. As a result of reduced resolution, there is a stronger overlapping between the activation areas of the individual contrast images. In contrast, the multiresolution approach preserves the anatomical specifics of the data, and nonlinear normalization methods have to be applied for group statistics.

In conclusion, wavelet-based multiresolution methods are generally more suitable for inference in fMRI than monoresolution filters. Using the general linear model, contrast images can be postprocessed in the wavelet domain by thresholding the wavelet coefficients and applying the Bonferoni correction method. In particular, if the smoothness and the location of the signal are unknown, wavelet-based methods avoid the problem of having to select the best monoresolution filter.

REFERENCES

1. Ruttimann UE, Unser M, Rawlings RR, et al. Statistical analysis of functional MRI data in the wavelet domain. IEEE Trans Med Imaging 1998;17:142–154.
2. Fadili MJ, Bullmore ET. Wavelet-generalized least squares: a new BLU estimator of linear regression models with 1/f errors. Neuroimage 2002;15:217–232.
3. Desco M, Hernandez JA, Santos A, Brammer M. Multiresolution analysis in fMRI: sensitivity and specificity in the detection of brain activation. Hum Brain Mapp 2001;14:16–27.
4. Brammer M. Multidimensional wavelet analysis of functional magnetic resonance images. Hum Brain Mapp 1998;6:378–382.
5. Bullmore E, Long C, Suckling J, et al. Colored noise and computational inference in neurophysiological (fMRI) time series analysis: resampling methods in time and wavelet domains. Hum Brain Mapp 2001;12:61–78.
6. Alexander ME, Baumgartner R, Summers AR, et al. A wavelet-based method for improving signal-to-noise ratio and contrast in MR images. Magn Reson Imaging 2000;18:169–180.
7. Alexander ME, Baumgartner R, Windischberger C, Moser E, Somorjai RL. Wavelet domain de-noising of time courses in MR image sequences. Magn Reson Imaging 2000;18:1129–1134.
8. Feilner M, Blu T, Unser M. Optimizing wavelets for the analysis of fMRI data. In: Proceedings of SPIE, vol. 4119. Conference on mathematical imaging: wavelet applications in signal and image processing VIII, San Diego, 2000. p 626–637.
9. Feilner M, Blu T, Unser M. Analysis of fMRI data using spline wavelets. In: Proceedings of the 10th European signal processing conference, Tampere, Finland, 2000. p 2013–2016.
10. LaConte SM, Ngan SC, Hu X. Wavelet transform-based Wiener filtering of event-related fMRI data. Magn Reson Med 2000;44:746–577.
11. Ngan SC, LaConte SM, Hu X. Temporal filtering of event-related fMRI data using cross-validation. Neuroimage 2000;11:797–804.
12. Raz J, Turetsky B. Wavelet ANOVA and fMRI. In: Proceedings of SPIE, vol. 3813. Wavelet applications in signal and image processing VII, Denver, 1999. p 561–570.
13. von Tscharner V, Thulborn KR. Specified-resolution wavelet analysis of activation patterns from BOLD contrast fMRI. IEEE Trans Med Imaging 2001;20:704–714.
14. Zaroubi S, Goelman G. Complex denoising of MR data via wavelet analysis: application for functional MRI. Magn Reson Imaging 2000;18:59–68.
15. Friston KJ, Holmes AP, Worsley KJ, Poline JP, Frith CD, Frackowiak RSJ. Statistical parametric maps in functional imaging: a general linear approach. Hum Brain Mapp 1995;2:189–210.
16. Worsley KJ, Friston KJ. Analysis of fMRI time-series revisited—again. Neuroimage 1995;2:173–181.
17. Friston KJ, Fletcher P, Josephs O, Holmes AP, Rugg MD, Turner R. Event-related fMRI: characterizing differential responses. Neuroimage 1998;7:30–40.
18. Zysset S, Müller K, Lohmann G, von Cramon DY. Color-word matching Stroop task: separating interference and response conflict. Neuroimage 2001;13:29–36.
19. Daubechies I. Ten lectures on wavelets. CBMS-NSF regional conference series in applied mathematics, vol. 61. Society for Industrial and Applied Mathematics, Philadelphia, 1992. 357 p.
20. Bultheel A. Learning to swim in a sea of wavelets. Bull Belg Math Soc 1995;2:1–45.
21. Mallat SG. A theory of multiresolution signal decomposition: the wavelet representation. IEEE Trans Pattern Anal Machine Intell 1989;11:673–693.
22. Press WH, Teukolsky SA, Vetterling WT, Flannery BP. Numerical recipes in C. Cambridge: Cambridge University Press; 1992. 994 p.
23. Donoho DL, Johnstone IM. Adapting to unknown smoothness via wavelet shrinkage. J Am Stat Assoc 1995;90:1200–1224.
24. Donoho DL, Johnstone IM. Ideal spatial adaption by wavelet shrinkage. Biometrika 1994;81:425–455.
25. Seber GAF. Linear regression analysis. New York: Wiley; 1977. 465 p.
26. Worsley KJ, Marrett S, Neelin P, Vandal AC, Friston KJ, Evans AC. A unified statistical approach for determining significant signals in images of cerebral activation. Hum Brain Mapp 1996;4:58–73.
27. Hawkins DM. Identification of outliers. London: Chapman and Hall; 1980.
28. Ugurbil K, Garwood M, Ellermann J, et al. Imaging at high magnetic fields: initial experiences at 4T. Magn Reson Q 1993;9:259–277.
29. Lee JH, Garwood M, Menon R, et al. High contrast and fast three-dimensional magnetic resonance imaging at high fields. Magn Reson Med 1995;34:308–312.
30. Norris DG. Reduced power multi-slice MDEFT imaging. Magn Reson Imaging 2000;11:445–451.
31. Lohmann G, Müller K, Bosch V, et al. Lipsia—a new software system for the evaluation of functional magnetic resonance images of the human brain. Comput Med Imaging Graph 2001;25:449–457.
32. James G. Advanced modern engineering mathematics. Harlow, England: Addison Wesley; 1999. 989 p.
33. Talairach P, Tournoux J. A stereotactic coplanar atlas of the human brain. Stuttgart: Thieme; 1988. 122 p.
34. Cox RW. AFNI: software for analysis and visualization of functional magnetic resonance neuroimages. Comput Biomed Res 1996;29:162–173.